CityU
香港城市大學
City University of Hong Kong
專業 創新 胸懷全球
Professional·Creative
For The World

CityU Scholars

Theoretical and Experimental Study of Nonlinear and Electro-Magneto-Mechanical-Based Piezoelectric Vibration Energy Harvester

Sun, Shilong; Zhang, Xiao

Published in:
Shock and Vibration

Published: 01/01/2019

Document Version:
Final Published version, also known as Publisher's PDF, Publisher's Final version or Version of Record

License:
CC BY

Publication record in CityU Scholars:
Go to record

Published version (DOI):
10.1155/2019/9093605

Publication details:
Sun, S., & Zhang, X. (2019). Theoretical and Experimental Study of Nonlinear and Electro-Magneto-Mechanical-Based Piezoelectric Vibration Energy Harvester. *Shock and Vibration*, *2019*, Article 9093605. https://doi.org/10.1155/2019/9093605

Citing this paper
Please note that where the full-text provided on CityU Scholars is the Post-print version (also known as Accepted Author Manuscript, Peer-reviewed or Author Final version), it may differ from the Final Published version. When citing, ensure that you check and use the publisher's definitive version for pagination and other details.

General rights
Copyright for the publications made accessible via the CityU Scholars portal is retained by the author(s) and/or other copyright owners and it is a condition of accessing these publications that users recognise and abide by the legal requirements associated with these rights. Users may not further distribute the material or use it for any profit-making activity or commercial gain.

Publisher permission
Permission for previously published items are in accordance with publisher's copyright policies sourced from the SHERPA RoMEO database. Links to full text versions (either Published or Post-print) are only available if corresponding publishers allow open access.

Take down policy
Contact lbscholars@cityu.edu.hk if you believe that this document breaches copyright and provide us with details. We will remove access to the work immediately and investigate your claim.

Download date: 14/05/2025

Hindawi
Shock and Vibration
Volume 2019, Article ID 9093605, 17 pages
https://doi.org/10.1155/2019/9093605

Research Article

Theoretical and Experimental Study of Nonlinear and Electro-Magneto-Mechanical-Based Piezoelectric Vibration Energy Harvester

Shilong Sun [1] **and Xiao Zhang** [2]

[1]*Department of Systems Engineering and Engineering Management, City University of Hong Kong, Hong Kong, China*
[2]*College of Computer Science, South-Central University for Nationalities, Wuhan, China*

Correspondence should be addressed to Xiao Zhang; xiao.zhang@my.cityu.edu.hk

Received 23 April 2019; Revised 8 September 2019; Accepted 3 October 2019; Published 11 November 2019

Academic Editor: Gianluca Gatti

Copyright © 2019 Shilong Sun and Xiao Zhang. This is an open access article distributed under the Creative Commons Attribution License, which permits unrestricted use, distribution, and reproduction in any medium, provided the original work is properly cited.

This paper presents a folded nonlinear electro-magneto-mechanical (EMM) vibration-based piezoelectric energy harvester system, which is built on the cantilevered beam structure and consists of one host beam and two substrate plates. The performance of the linearity and nonlinearity to the proposed EMM system is evaluated and compared. Moreover, the voltage response in time history and the phase portrait are studied under an external rectifier circuit with a resistor. The results show that the nonlinearity of the reported EMM system changes the coherent resonance vibration mode from single to double under a harmonic base excitation within the frequency range of 20 Hz–50 Hz. Meanwhile, the substrate plate D contributes more averaged voltage output at a lower frequency while the substrate plate A contributes the voltage output at the relatively higher frequency for the nonlinear EMM system. The experimental study indicates that the proposed nonlinear EMM vibration-based piezoelectric energy harvester can yield a total voltage of 8.133 V@35.53 Hz while the baseline structure only produces 1.724 V@38.81 Hz. In addition, the bandwidth range of high-power output is enlarged by the nonlinear EMM system, which makes this device more flexible and applicable to absorb the wasted vibration energy generated by industrial machines and public facilities.

1. Introduction

Recently, the concepts of smart city and smart life have been attracting increasingly more attention by researchers and industry practitioners. Wireless sensor networks (WSNs) play an important role in achieving these green energy device designs [1]. However, the power source of WSNs limits its practical applications, such as the implementation of the public buildings and low-frequency vibrating rotational machines [2]. A smart device of vibration-based piezoelectric energy harvester is a key alternative method to address this issue [3]. The vibration from the rotational machine is one of the most common mechanical energy, especially in the buildings and factories [4]. Generally, all generated vibrations are destructive as they may make the structure/component to oscillate and vibrate. In other words, waste vibration has the same meaning as destructive vibration. Excessive movements will cause the components to wear out and dislocate. By minimizing the vibration generated by one component that may pass to adjacent components, the adjacent components may vibrate less and last longer in their service lives. The vibration frequency from the rotational machine is usually small and harmful to the lifespan of the machines. Therefore, it is essential to design a device which not only reduces the destructive vibration but also collects the wasted vibration energy [5, 6].

The traditional energy harvester based on mechanical vibration has some typical drawbacks, like the narrow

bandwidth and lower energy efficiency. These shortcomings limit and block the high-power generation and make it difficult for the implementation of such kinds of devices into the real practical engineering applications, like the low-frequency rotational machines [7, 8]. Therefore, matching the resonance frequency of energy harvester with the rotational machine's vibrating frequency is an effective approach. The rotational machines have their specific frequencies range when they are vibrating. The energy harvester device installed on the rotary machines can achieve its maximum power output around its vibrating resonance frequency. A well-known low-frequency mechanism called X-stable configuration has been widely investigated in broadening the frequency range of the vibration-based piezoelectric energy harvester in past few years, such as the bistable [9, 10], tristable [11, 12], quadstable [13, 14], and multistable [15, 16] systems. The bistable configuration attaching the nonlinearity can achieve its high energy output and broaden the frequency performance through its motion on high orbit. The tristable model has a relationship with the locations of tip and magnets but without significant improvement upon the energy output density [17]. The shapes of the quadstable structures compared with the bistable and tristable ones are adverse to the energy conversion efficiency.

The nonlinearity coupled with the magnetic materials can broaden the frequency bandwidth of energy harvester further [18, 19]. The nonlinearity can be used to enlarge resonant bandwidth of vibration energy harvester with piezoelectric cantilevered beams [20]. The multi-degree-of-freedom (DOF) energy harvester model can provide the multiple close resonance vibration peaks over a wide frequency bandwidth [21, 22], which facilitate its application in an unstable and variable ambient environment, especially for the variable-frequency devices. Čeponis and Mažeika [23] investigated a multi-frequency piezoelectric energy harvester by using arrays of simple cantilever beams. This kind of design increased structural complication and space occupation. The combination of the magnetic material with the multiple-degree-of-freedom can efficiently improve system performance further, including the bandwidth and the amplitude of the power output [24]. However, it is hard to design a model with a compacted multi-degree-of-freedom structure coupled with the magnetic interaction, because its dynamic performance cannot be calculated directly due to the complicated structure parameters. To fill this void in current research work, a folded nonlinear electro-magneto-mechanical (EMM) vibration-based piezoelectric energy harvester model is proposed in this paper.

This paper is organized as follows: In Section 2, the nonlinear EMM vibration-based piezoelectric energy harvester aluminum model and the derivation of mathematical governing motion equations are briefly introduced. The equivalent model of the EMM system is built up, and the system dynamic motion equations are derived based on this equivalent model. Section 3 describes the experimental setup, fabrication, and tests of the EMM vibration-based piezoelectric energy harvester. Section 4 presents the analysis of the resonance frequency. Section 5 provides the dynamic response behavior under the linear and nonlinear EMM model, including the resonance vibration mode, the voltage in time history, the phase portrait, and the experimental voltage. Section 6 compares the voltage generated on the different plates. The summaries are given in Section 7.

2. Design and Modeling Analysis

The definition of the linear system is that there is not any repelling force or magnetic force, or any other mutual forces between the block A and block D shown in Figure 1. For the nonlinear system, the block A and block D were replaced by two permanent magnets with the same size and weight but opposite direction and the repulsive force between the two magnets would drive the two substrate plates vibrating in a nonlinear dynamic style under a given basis excitation.

Figure 1 shows the schematic diagram of the proposed nonlinear electro-magneto-mechanical system. This nonlinear EMM system is composed of one cantilevered host beam and two substrate plates with the same rectangular permanent magnets as tip mass. The two substrates plate are assumed and made of the piezoelectric material. The rectangular tip mass is composed of the permanent magnet or the iron block. If the permanent magnet is made of the tip mass, then the EMM system is nonlinear. If the rectangular tip mass is replaced with the same dimension and mass of the iron block, then there is no repulsive force between the tip masses and this multiple-degree-of-freedom EMM piezoelectric vibration energy harvester system becomes linear.

The two substrate plates have the same geometric and material composition. The driving excitation frequency is set from 20 Hz to 50 Hz to make this device more flexible and applicable to implement on the industrial machine and public facilities because most of the industrial machine frequencies are under the range of 20 Hz to 50 Hz.

The substrate plates A and D are composed of the piezoelectric layer. Each substrate plate can vibrate at its resonance frequency. The substrate plate A has one sharp lower single-resonance frequency with a narrow range output. The substrate plate D coupling with the host beam is a compact folded cantilevered design with a wider bandwidth. Both the settings are connected to a rectifier with a capacitor in series to make the whole system cover a wider bandwidth. When the permanent magnets are placed in an opposite direction, the repulsive force between the two magnets would drive the two substrate plates vibrating under a given basis excitation. By using the repulsive force, the strains on the substrate plates A and D will be enhanced compared to the tip mass made by iron block without the permanent magnets. Here, the horizontal

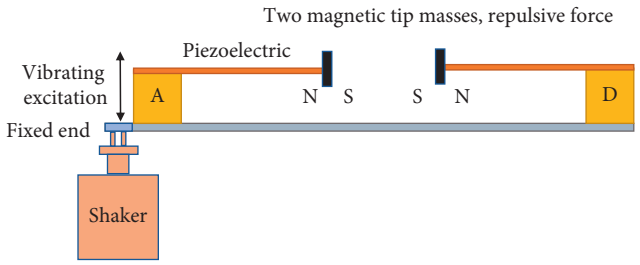

Figure 1: Schematic diagram of the nonlinear and EMM harvester.

distance between the magnets is assumed to be a constant when the system is vibrating, since the deflection on the free end of substrate plates is much smaller, compared to that length of the plates.

As introduced before, there is a repulsive force between the two permanent magnets. It is also a time-varying force because of the positions changing along with the system vibration. Figure 2 shows the dimensions of the rectangular permanent magnets, and Figure 3 displays the detailed geometric diagram between the two rectangular permanent magnets at the relative position. Table 1 shows the dimensions of the magnets.

Because the magnet is assumed as the rectangular one, then the repulsive force between them can be calculated by the following equation [25, 26]:

$$F_m = w_B l_B h_B^n B_r |B(d)| f(d), \tag{1}$$

where w_B, h_B and l_B are the width, thickness, and length of the rectangular permanent magnet, respectively; $n = 1/3$ and B_r is the residual flux density of the magnet; $B(d)$ is the magnitude of the magnetic flux density field; and $f(d)$ is an empirical function which is used to express the degradation of the repelling force between two magnets [27]:

$$|B(d)| = \frac{B_r}{\pi}\left[\tan^{-1}\left(\frac{w_B l_B}{2d\sqrt{w_B^2 + l_B^2 + 4d^2}}\right) - \tan^{-1}\left(\frac{w_B l_B}{2(h_B + d)\sqrt{w_B^2 + l_B^2 + 4(h_B + d)^2}}\right)\right],$$

$$f(d) = \left(1.749 + 1.145e^{(-(d/d_0))}\right) \times 10^6 \left(\mathrm{NT}^{-2}\mathrm{m}^{-(7/3)}\right). \tag{2}$$

For the nonlinear system, there is a repulsive force between the two permanent magnets and the directions of this force can be decomposed by one horizontal direction and one vertical direction; therefore, the options of the magnets can be assumed as a circular motion. Since the lengths of plate A and plate D are far larger than the displacement of the tip mass, the plate A and plate D vibration can be assumed as a circular motion with the time varying at a radius of $L + 0.5h_B$.

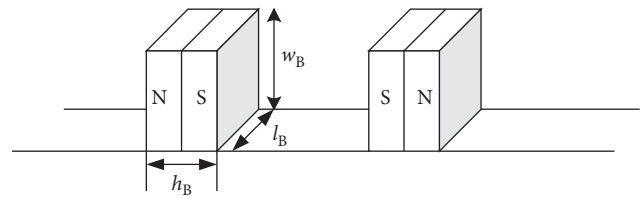

Figure 2: Dimensions of rectangular permanent magnets.

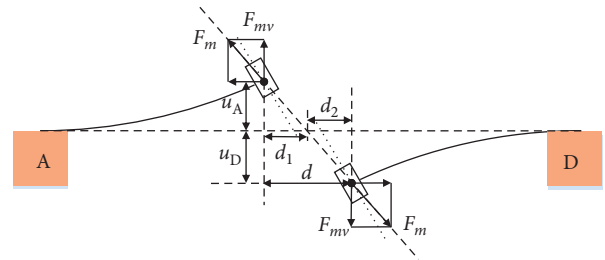

Figure 3: Geometric diagram between the two rectangular permanent magnets at the relative position.

Table 1: Dimensions of the magnets.

Description	Parameter	Value	Unit
Magnet length	l_B	0.03	m
Magnet width	w_B	0.01	m
Magnet thickness	h_B	0.003	m
Residual flux density	B_r	0.005	T
Original distance between permanent magnets	d	0.002	m

Then, the magnetic force can be expressed as

$$F_m = \frac{w_B l_B h_B^{1/3} B_r^2}{\pi}\left[\tan^{-1}\left(\frac{w_B l_B}{2d\sqrt{w_B^2 + l_B^2 + 4d^2}}\right) - \tan^{-1}\left(\frac{w_B l_B}{2(h_B + d)\sqrt{w_B^2 + l_B^2 + 4(h_B + d)^2}}\right)\right] f(d), \tag{3}$$

$$F_{mv} = F_m \times \frac{u_A - u_D}{\sqrt{(u_A - u_D)^2 + d^2}}. \tag{4}$$

To simplify the computational complexity, we define the $u_A - u_D$ like the following equation:

$$y_{AD} = u_A - u_D. \tag{5}$$

The binomial series was used to redefine equation (4) as [25]

$$F_{mv} = F_m \times \left(\frac{y_{AD}}{d} - \frac{y_{AD}^3}{2d^3}\right). \tag{6}$$

The repulsive magnetic force in the same direction with the excitation motion can be denoted as F_{mv}. It is perpendicular to the horizontal beam direction. Figure 4 shows the equivalent model of the proposed electro-magneto-mechanical system.

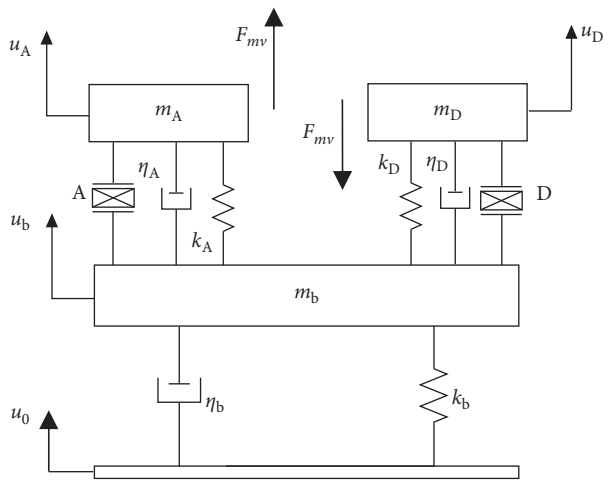

FIGURE 4: Equivalent model of the proposed electro-magneto-mechanical system.

Therefore, the general governing equations of the EMM system can be written as [21, 28].

$$\begin{cases} m_A\ddot{u}_A = -\eta_A(\dot{u}_A - \dot{u}_b) - k_A(u_A - u_b) - \theta V_{pA} - F_{mv}, \\ m_D\ddot{u}_D = -\eta_D(\dot{u}_D - \dot{u}_b) - k_D(u_D - u_b) - \theta V_{pD} + F_{mv}, \\ m_b\ddot{u}_b = -\eta_b(\dot{u}_b - \dot{u}_0) - k_b(u_b - u_0) + [\eta_A(\dot{u}_A - \dot{u}_b) \\ \quad + k_A(u_A - u_b) + \theta V_{pA}] + [\eta_D(\dot{u}_D - \dot{u}_b) + k_D(u_D - u_b) \\ \quad + \theta V_{pD}] - \theta\dot{y}_A + C^S\dot{V}_{pA} + \dfrac{V_{pA}}{R_L} = 0 - \theta\dot{y}_D + C^S\dot{V}_{pD} \\ \quad + \dfrac{V_{pD}}{R_L} = 0, \end{cases} \tag{7}$$

where u_A, u_D, and u_b are the relative displacement of the tip mass on the substrate plate A, the substrate plate D, and the host beam. $u_0 = A_0 \sin(\omega t)$ is the base sinusoidal excitation. θ denotes the electromechanical effect coefficient. $V_p(t)$ denotes the output voltage of the piezoelectric. C^S denotes the clamped capacitance of the piezoelectric. m and k denote the damping mass and the stiffness of the electromechanical system. F_{mv} is the magnetic force applied along the transverse direction of the aluminum beam. The subscripts A, D, and b denote the substrate plate A, the substrate plate D, and the aluminum beam.

Giving the following definition

$$\begin{cases} y_A = u_A - u_b, \\ y_D = u_D - u_b, \\ y_b = u_b - u_0. \end{cases} \tag{8}$$

Then, equation (7) can be reorganized as

$$\begin{cases} m_A\ddot{y}_A + \eta_A\dot{y}_A + k_A y_A + \theta V_{pA} + F_{mv} = -m_A\ddot{y}_b - m_A\ddot{u}_0, \\ m_D\ddot{y}_D + \eta_D\dot{y}_D + k_D y_D + \theta V_{pD} - F_{mv} = -m_D\ddot{y}_b - m_D\ddot{u}_0, \\ (m_A + m_D + m_b)\ddot{y}_b + \eta_b\dot{y}_b + k_b y_b + m_A\ddot{y}_A + m_D\ddot{y}_D \\ \quad + (m_A + m_D + m_b)\ddot{u}_0 = 0 - \theta\dot{y}_A + C^S\dot{V}_{pA} + \dfrac{V_{pA}}{R_L} = 0 \\ \quad - \theta\dot{y}_D + C^S\dot{V}_{pD} + \dfrac{V_{pD}}{R_L} = 0. \end{cases} \tag{9}$$

We give the definition $\omega_A = \sqrt{k_A/m_A}$, $\omega_D = \sqrt{k_D/m_D}$, $\omega_b = \sqrt{k_b/m_b}$, $\zeta_D = \eta_D/2\sqrt{k_D m_D}$, $\zeta_b = \eta_b/2\sqrt{k_b m_b}$, $\mu = m_A/m_b = m_D/m_b$; then, equation (9) becomes

$$\begin{cases} \ddot{y}_A + 2\zeta_A\omega_A\dot{y}_A + \omega_A^2 y_A + \theta\dfrac{V_{pA}}{m_A} + \dfrac{F_{mv}}{m_A} = -\ddot{y}_b - \ddot{u}_0, \\ \ddot{y}_D + 2\zeta_D\omega_D\dot{y}_D + \omega_D^2 y_D + \theta\dfrac{V_{pD}}{m_D} - \dfrac{F_{mv}}{m_D} = -\ddot{y}_b - \ddot{u}_0, \\ (1 + 2\mu)\ddot{y}_b + 2\zeta_b\omega_b\dot{y}_b + \omega_b^2 y_b + \mu\ddot{y}_A + \mu\ddot{y}_D \\ \quad + (1 + 2\mu)\ddot{u}_0 = 0 - \theta\dot{y}_A + C^S\dot{V}_{pA} + \dfrac{V_{pA}}{R_L} = 0 - \theta\dot{y}_D \\ \quad + C^S\dot{V}_{pD} + \dfrac{V_{pD}}{R_L} = 0. \end{cases} \tag{10}$$

In order to solve equation (10), the state space form is defined as [10]

$$\begin{aligned} &[q(1)\ q(2)\ q(3)\ q(4)\ q(5)\ q(6)\ q(7)\ q(8)]^T \\ &= [y_A\ \dot{y}_A\ y_D\ \dot{y}_D\ y_b\ \dot{y}_b\ V_{pA}\ V_{pD}]^T. \end{aligned} \tag{11}$$

Then, equation (11) can be reorganized as

$$\begin{bmatrix} \dot{q}(1) \\ \dot{q}(2) \\ \dot{q}(3) \\ \dot{q}(4) \\ \dot{q}(5) \\ \dot{q}(6) \\ \dot{q}(7) \\ \dot{q}(8) \end{bmatrix} = \begin{bmatrix} q(2) - 2\zeta_{\mathrm{A}}\omega_{\mathrm{A}}q(2) - \omega_{\mathrm{A}}^2 q(1) - \theta\dfrac{q(7)}{m_{\mathrm{A}}} - \dfrac{F_{mv}}{m_{\mathrm{A}}} - \dot{q}(6) - \ddot{u}_0 \\ q(4) - 2\zeta_{\mathrm{D}}\omega_{\mathrm{D}}q(4) - \omega_{\mathrm{D}}^2 q(3) - \theta\dfrac{q(8)}{m_{\mathrm{D}}} + \dfrac{F_{mv}}{m_{\mathrm{D}}} - \dot{q}(6) - \ddot{u}_0 \\ q(6) - \dfrac{1}{(1+2\mu)}\left(2\zeta_{\mathrm{b}}\omega_{\mathrm{b}}q(6) + \omega_{\mathrm{b}}^2 q(5) + \mu\dot{q}(2) + \mu\dot{q}(4)\right) - \ddot{u}_0 \\ \dfrac{\theta}{C^S}q(2) - \dfrac{q(7)}{R_{\mathrm{L}}C^S} \\ \dfrac{\theta}{C^S}q(4) - \dfrac{q(8)}{R_{\mathrm{L}}C^S} \end{bmatrix}. \tag{12}$$

Since this equation expresses a first-order ordinary differential equation with the time dependency, the numerical solution is needed to solve equation (12) based on the harmonic excitation assumption. The solver of Runge–Kutta methods in MATLAB is used to solve the first-order ordinary differential equations. Table 2 shows the parameters used in the theoretical study of the equivalent model.

To study the maximized power output, an external circuit design was applied to the proposed electro-magneto-mechanical system. The voltage generated by the electro-magneto-mechanical piezoelectric vibration energy harvester is an alternating current signal; the circuit is designed and used to convert the AC to DC signal.

Solving equation (12), the total voltage response of the proposed electro-magneto-mechanical system is

$$V_{\mathrm{p}} = V_{\mathrm{pA}} + V_{\mathrm{pD}}, \tag{13}$$

where V_{pA} denotes the voltage collected on the A piezoelectric material and V_{pD} denotes the voltage collected on the D piezoelectric material. The total voltage response is the sum of these two subcomponent voltages V_{pA} and V_{pD}.

Both the settings are connected to a rectifier with a capacitor and a 1 MΩ external resistor load, and then, the output power response can be obtained as

$$P = \frac{\left(V_{\mathrm{pA}} + V_{\mathrm{pD}}\right)^2}{R_{\mathrm{L}}}. \tag{14}$$

3. Experiment Setup and Model Fabrication

To validate the nonlinear wideband piezoelectric energy harvester's performance and investigate its dynamic characteristics, the experimental research is conducted and the electric circuit design is utilized to study the electric energy output. The configuration is fabricated and tested by the wood, the aluminum beam, and the rectangular permanent magnets. Figure 5 shows the schematic of the experimental setup, which is used to validate the results generated from the numerical analysis. The system is composed of the function generator, the Pulse Labshop, the power amplifier, the external circuit, and the B&K shaker. The piezoelectric materials are the Quick Pack Model which is manufactured by the Mide Technology Corporation. The excitation frequency range is set up to from 20 Hz to 50 Hz. The voltage response and resonance frequency are measured by the Pulse Labshop software which is installed on a computer. The parameters of the equivalent model are shown in Table 2. The external resistor was set up to 1 MΩ because the transferred power is the highest at this resistor.

Figure 6 shows the experimental and configuration setup. The results from the baseline structure and the designed structure are compared to evaluate the ability to convert and storing the electrical energy.

4. Analysis of the Resonance Frequency

This paper focuses on the performance of the EMM system for both linear and nonlinear systems. The voltage in time history analysis and the effect of residual flux density are studied in this section. Here, the toolbox function "ode45" provided by MATLAB is used to solve equation (12) and obtain the voltage in time history and the phase portrait. The linear EMM system was defined as the residual flux density B_{r} equal to 0. If the B_{r} is set up to 0.000 T, then there is no magnetic force applied to this EMM system, which means this kind of system is performed as a linear response. For the nonlinear EMM system, the value of B_{r} is set as 0.005 T. The original distance d between the two magnets is set to 0.002 m. The voltage in time history and the phase portrait are studied under the residual flux density which is set up to 0.000 T and 0.005 T, respectively.

Figure 7 shows the analysis of the resonance frequency for the linear and nonlinear system. According to Figure 7, there is only one resonant vibration mode of the linear EMM system between the frequencies range from 20 Hz to 50 Hz, and the first resonance frequency is 28 Hz. However, for the nonlinear EMM system with a $B_{\mathrm{r}} = 0.005$ T as shown in Figure 7(b), there are two resonance frequencies which are 23 Hz and 33 Hz, respectively, at the same frequency range. More resonance vibration modes mean that the maximum power output can be obtained. Therefore, there is an advantage for the power output of the nonlinear EMM system when compared to the linear one, theoretically.

Table 2: Parameters of the equivalent model.

Description	Parameter	Value	Unit
Equivalent stiffness of the substrate plate A, substrate plate D, and host beam	k_A	16	N/m
	k_D	10	N/m
	k_b	400	N/m
Equivalent mechanical damping of the substrate plate A, substrate plate D, and host beam	η_A	0.0064	Ns/m
	η_D	0.00512	Ns/m
	η_b	0.8	Ns/m
Equivalent mass of the substrate plate A, substrate plate D, and the host beam	$m_A = m_D$	40	g
	m_b	1000	g
Amplitude of the base sinusoidal excitation	A_0	0.005	m
Electromechanical effect coefficient	θ	0.001	N/V
Clamped capacitance of the piezoelectric	C^S	50.2	nF
External resistor load	R_L	1	MΩ

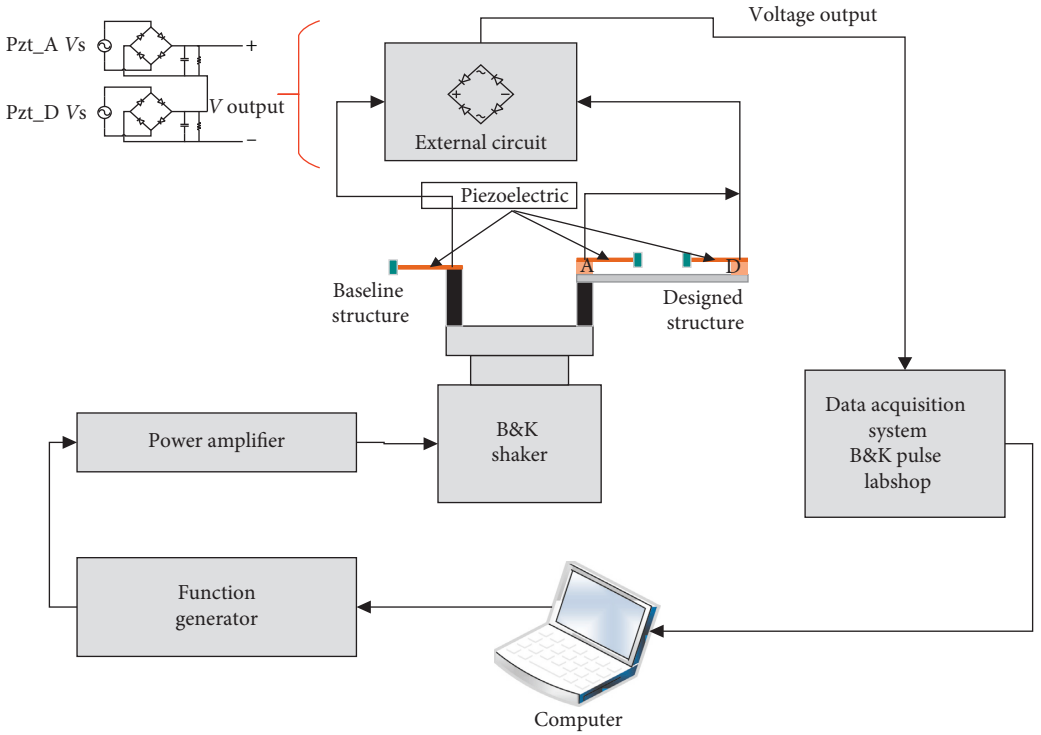

Figure 5: Schematic of the experimental setup.

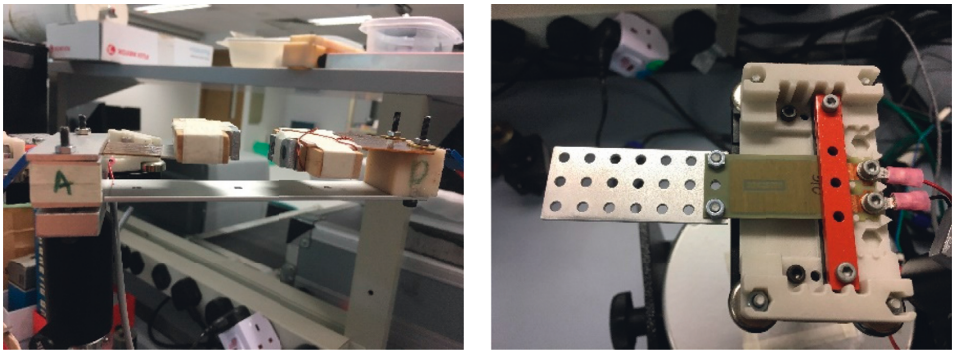

(a) (b)

Figure 6: Continued.

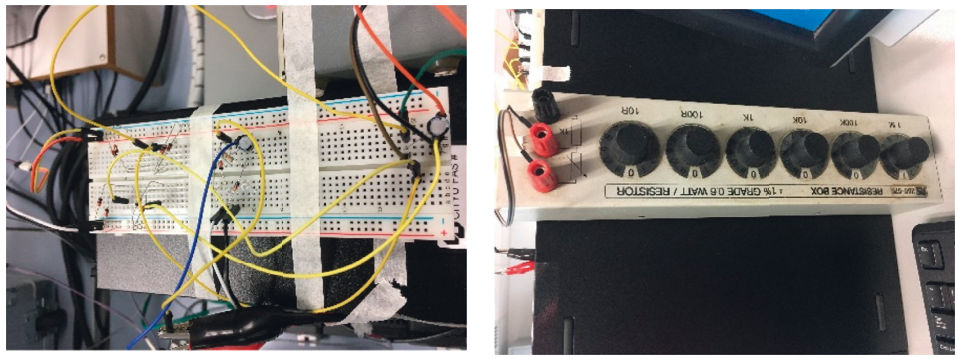

(c) (d)

Figure 6: Experiment and the configuration setup: (a) the designed structure; (b) the baseline structure; (c) the electric circuit; (d) the external resistor.

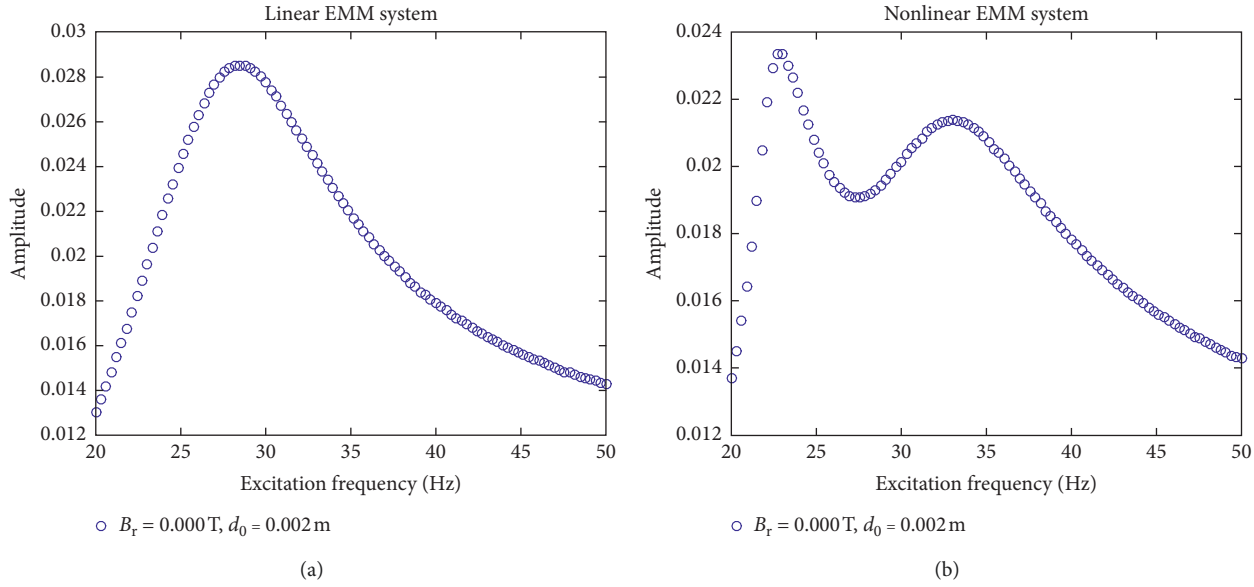

(a) (b)

Figure 7: Analysis of the resonance frequency on the (a) linear and (b) nonlinear system.

In this work, after adding the nonlinearity to the linear system, the single resonant vibration mode becomes two resonant vibration modes as shown in Figure 7. More resonant vibration modes mean more peak power output. However, the practical maximum power output, which is slightly complicated due to multiple factors, such as the resonance frequency and the resistors. To investigate the real power output, 23 Hz, 28 Hz, and 33 Hz are selected to be taken as the three base resonance frequencies. The performance and the dynamic characteristic of both EMM systems are compared and studied in Sections 5 and 6.

5. Comparison of the Linear and Nonlinear EMM System

5.1. Analysis of the Voltage-Time and Phase Portrait for Linear System. As introduced before, the linear EMM system is defined according to the residual flux density is assumed to be equal to 0. The distance between the two tip masses is equal to 0.002 m. The voltage performance in time history and the phase portrait at the frequency of 23 Hz, 28 Hz, and 33 Hz are shown in Figure 8. The voltage response is collected at the time of one second in time history analysis. The red line represents the host beam, the blue line denotes the substrate plate A, and the green line denotes the substrate plate D. All the lines shown in the following figures have the same definitions.

Figure 8 shows the voltage in time history and the phase portrait of the linear EMM system. To show the voltage response clearly, only a time trend of one second is plotted in Figures 8(a), 8(c), and 8(e). The phase portrait is plotted in Figures 8(b), 8(d), and 8(f) and has a record time of 100 seconds. It is because the stable orbit of the dynamic is needed to demonstrate that this structure can be run in balance and smoothly. From the phase portrait at the frequency of 23 Hz, 28 Hz, and 33 Hz, the motion orbit of plates

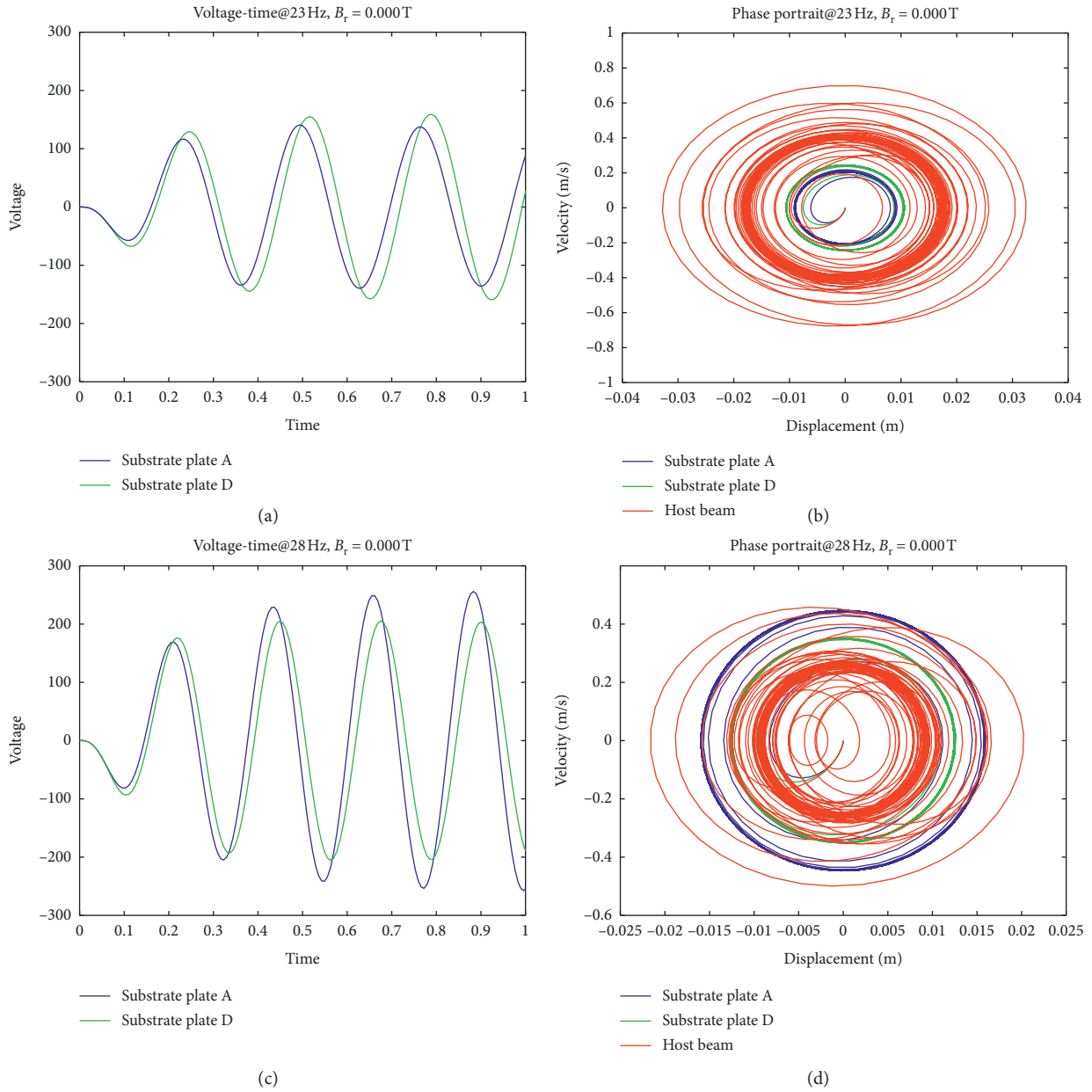

Figure 8: Continued.

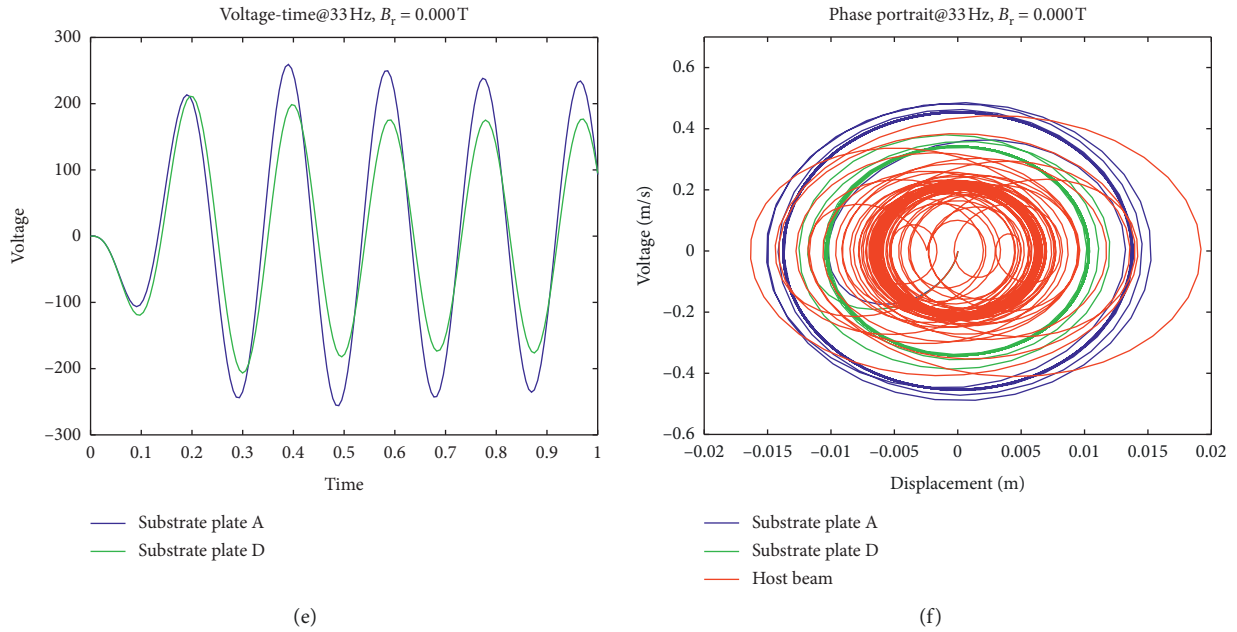

Figure 8: Voltage in time history and the phase portrait for the linear EMM system: (a) voltage-time@23 Hz; (b) phase portrait@23 Hz; (c) voltage-time@28 Hz; (d) phase portrait@28 Hz; (e) voltage-time@33 Hz; (f) phase portrait@33 Hz.

A and D has a large amplitude and the orbits are stable at the frequency of 28 Hz which means they could produce the highest mechanic energy at the frequency of 28 Hz compared to the other two frequencies. The reason is that the frequency of 28 Hz is the only resonance frequency for this linear EMM system which has the largest mode deflection and mechanical strain. Also, the dynamic orbit is in a balance high orbit for both the two plates. The velocity value of the substrate plate A is smaller than that of the substrate plate D at 23 Hz. For the other frequencies, the amplitude of the velocity exhibits an opposite trend which shows the velocity of the plate A is larger than that of the plate D.

Tables 3 and 4 provide the quantitative values of the averaged voltage, the averaged velocity, and the averaged displacement of the linear EMM system. From Table 5, the averaged voltage of the substrate plate A is 85.355 mV at 23 Hz while that of the substrate plate D is 100.439 mV at 23 Hz. It can be observed that the substrate plate D contributes more energy than the substrate plate A at 23 Hz. However, the averaged voltage of the substrate A is 165.1822 mV at 28 Hz while that of the substrate plate D is 128.2923 mV at 28 Hz. The voltage on plate A is larger than that of the plate D which is an opposite trend with the voltage response at 23 Hz. The voltage at 33 Hz has the same performance in comparison with the 28 Hz, which shows the voltage on the plate A is larger than that of the plate D. Consequently, the substrate plate A works well at the lower frequency, and the substrate plate D contributes more at the larger frequency. Another conclusion is that the total voltage obtained at 28 Hz is larger than the other two frequencies' voltages because 28 Hz is the only resonance frequency during the range of 20 Hz–50 Hz for the linear EMM system.

Table 3: Averaged displacement (m) of the linear EMM system in 100 seconds.

	23 Hz	28 Hz	33 Hz
Substrate plate A	0.0057	0.0101	0.0087
Substrate plate D	0.0067	0.0079	0.0065
Host beam	0.0113	0.006	0.0041

Table 4: Averaged velocity (m/s) of the linear EMM system in 100 seconds.

	23 Hz	28 Hz	33 Hz
Substrate plate A	0.1327	0.2865	0.2935
Substrate plate D	0.1549	0.2247	0.2221
Host beam	0.2589	0.1642	0.1383

Table 5: Averaged voltage (mV) of the linear EMM system in 100 seconds.

	23 Hz	28 Hz	33 Hz
Substrate plate A	85.355	165.1822	150.8015
Substrate plate D	100.439	128.2923	112.9848
Total	185.794	293.4745	263.7863

The averaged displacement and the averaged velocity of the linear system were recorded in 100 seconds. These two parameters have demonstrated and supported the dynamic performance of the averaged voltage of the linear EMM system. The displacement of plate A is 0.0087 m at 33 Hz while the displacement of plate D is 0.0065 m at the same frequency. However, no matter the plate A or the plate D,

both their averaged displacements at 28 Hz are larger than the other frequencies' displacements.

Figure 9 shows the power output in time history for the linear EMM system. The resonant vibration frequency is 28 Hz; therefore, the power output for the linear EMM system has the highest values at 28 Hz. The power phase for the substrate plate A is a little earlier than that of the substrate plate D at 28 Hz, and the value is also large than the power on plate D. From the point of phase angle, it is convenient to collect the energy around the peak point if the plate can achieve its resonant vibration mode at a lower frequency. It only occurs at the frequency of 23 Hz which shows the power output on substrate plate D is larger than that on substrate plate A. For the other two frequencies, the power on plate A is larger than that of plate D. Hence, for the linear EMM system, the substrate plate D works efficiently at a lower frequency range while the substrate plate A works efficiently at a higher frequency range.

5.2. Analysis of the Voltage-Time and Phase Portrait for the Nonlinear System. For the nonlinear EMM system, the residual flux density of the magnets is defined as 0.005 T. The interaction between the magnets can produce the nonlinearity effect of the whole structure, because of the repulsive magnetic forces. The original distance between the permanent magnets is 0.002 m. The magnetic force is produced between the permanent magnets, and its decomposition in excitation direction becomes variable when the distance changes. That is because the deflection on the free end of the substrate plates A and D changes. The detailed dynamic analysis of the repulsive forces has been provided in Figure 3, and the mathematical equations also have been derived according to equations (4)–(6).

Figure 10 shows the voltage response in time history and the phase portrait of the nonlinear EMM system. Similar to the linear EMM system, the voltage response is recorded in 1 second, and the phase portrait is plotted in 100 seconds. As shown in Table 6, the averaged voltage of the substrate plate A is 104.8723 mV@23 Hz, 110.7777 mV@28 Hz, and 133.7134 mV@33 Hz. The averaged voltage of the substrate plate D is 122.007 mV@23 Hz, 86.4744 mV@28 Hz, and 99.6883 mV@33 Hz. Therefore, the averaged voltage at 23 Hz and 33 Hz is larger than that of 28 Hz for both the plate A and the plate D except the voltage of plate A at 23 Hz is slightly lower than that of 28 Hz. However, the total voltages for both plates at corresponding frequencies are higher than the whole voltage at 28 Hz. The reason is that due to the nonlinearity to the EMM system, the resonance vibration mode becomes two resonant vibration modes from single resonant vibration mode during the frequency range of 20 Hz–50 Hz, and then the power outputs at the two resonance frequencies should be larger than any other particular frequency.

Figures 10(b), 10(d), and 10(f) show the phase portrait at the frequency of 23 Hz, 28 Hz, and 33 Hz. The motion orbits of the substrate plate A and the substrate plate D exhibit an opposite trend at the first resonant vibration mode and the second resonant vibration mode. The motion orbit of the substrate plate D is larger than that of the substrate plate A at the frequency of 23 Hz and the substrate plate A is larger than that of the substrate plate D at 33 Hz. The larger amplitude the motion orbit, the more energy the tip mass produced. This performance also agrees with the averaged voltage response as already demonstrated in Figures 10(a), 10(c), and 10(e).

As observed from Tables 7 and 8, the performance of the two subplates appears with the opposite trends of the deflection on each of the free end. The first resonant mode of 23 Hz yields a large deflection of the substrate plate D and small deflection of the substrate plate A. However, for the second resonant mode of 33 Hz, it has small deflection of substrate plate D and large deflection of substrate plate A. For the substrate plate A and substrate plate D, the averaged displacement of plate A is 0.0068 m which is lower than that of the plate D is 0.0079 m at the frequency of 23 Hz. This means the deflection of plate D is larger than plate A at the frequency of 23 Hz, and it contributes more energy to the whole system at this moment. As the excitation frequency increased to 28 Hz and 33 Hz, the displacement of the plate A is larger than that of the plate D at both two frequencies which mean the plate A dominates the main mechanical energy to the nonlinear EMM system at higher excitation frequencies. The higher the displacement, the larger the system mechanical strains.

As given in Table 8, the host beam generates the highest averaged velocity of 0.2437 m/s while the substrate plate A is 0.1568 m/s and the substrate plate D is 0.1898 m/s. At the frequency of 28 Hz, the averaged velocity of the substrate plate A is 0.1925 m/s which is larger than the substrate plate D of 0.15 m/s and the host beam of 0.16 m/s. At the frequency of 33 Hz, the averaged velocity of the substrate plate A is 0.2607 m/s which is the largest among these three components of the whole system while the averaged velocity of the substrate plate D is 0.1977 m/s and the host beam of 0.1433 m/s. The higher the averaged velocity, the larger the mechanical energy of the system. In conclusion, for the two resonance frequencies of 23 Hz and 33 Hz, the substrate plate D dominates more energy at first resonance frequency 23 Hz while the substrate plate A dominates more energy at the second resonance frequency 33 Hz. Both are larger than the averaged velocity at 28 Hz because of the resonant vibration mode effect.

Figure 11 shows the power output in time history for the nonlinear EMM system. From Figure 11(a), the substrate plate A always achieved its power peak than that of the substrate plate D and the phase of power output is a little earlier than that of the substrate plate D. However, the levels of the power output levels for the substrate plate D are larger than the substrate plate A at 23 Hz. For the frequency of 28 Hz and 33 Hz, the piezoelectric on the substrate plate A dominates the power output than the substrate plate D. Therefore, the substrate plate D works efficiently at a lower

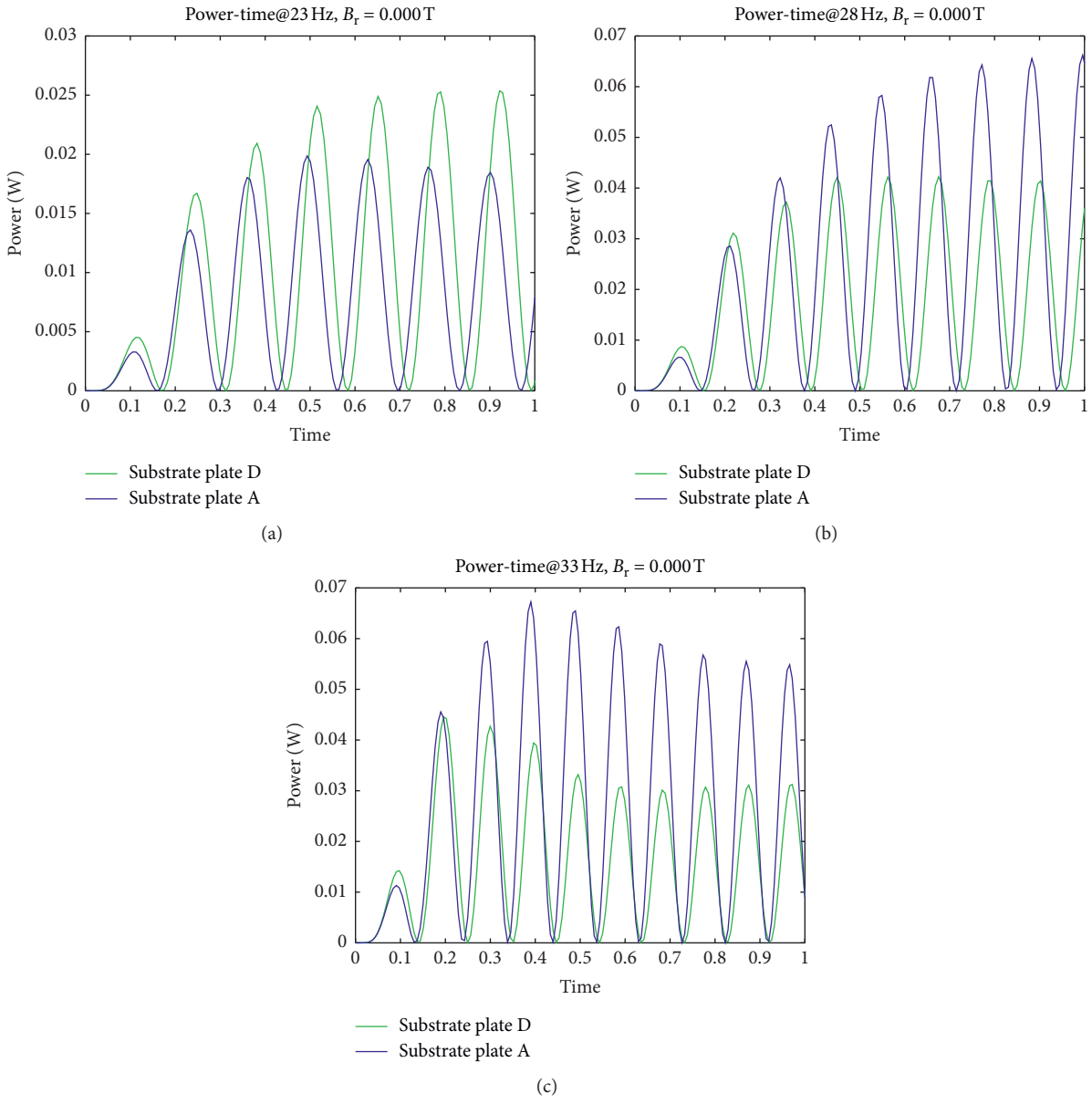

Figure 9: Power output in time history for the linear EMM system: (a) 23 Hz; (b) 28 Hz; (c) 33 Hz.

frequency (23 Hz) while the substrate plate A works efficiently at higher frequency (28 Hz and 33 Hz).

6. Comparison of the Voltage Generated by Piezoelectric on Plate A and Plate D

To validate the priority of the proposed structure, the designed structure and the baseline structure are compared and studied. The components of the baseline structure mainly come from the Mide Company. The designed structure and the baseline structure are placed on the experimental platform and given the same external simulated excitation, and the voltage response is observed and investigated for both structures. Figures 12–14 demonstrate the voltage response between the piezoelectric on substrate plate A, the piezoelectric on substrate plate D, the piezoelectric on substrate plates A and D and the baseline structure, respectively.

The maximum voltage point is obtained at 23.6 Hz with a peak value of 1.729 V while the voltage on the baseline structure obtained its peak value of 1.726 V@ 38.76 Hz. It can be concluded that the piezoelectric on the substrate plate A contributes more energy when the ambient environment frequency is small. It will achieve the resonance frequency at an early-stage life cycle of the machines. However, the energy generated on piezoelectric on substrate plate A contributes little energy for the whole structure power output in comparison with the piezoelectric on the substrate plate D. The maximum voltage for the piezoelectric on substrate plate D is 8.078 V@35.56 Hz while the piezoelectric on substrate plate A is 1.729 V@23.6 Hz.

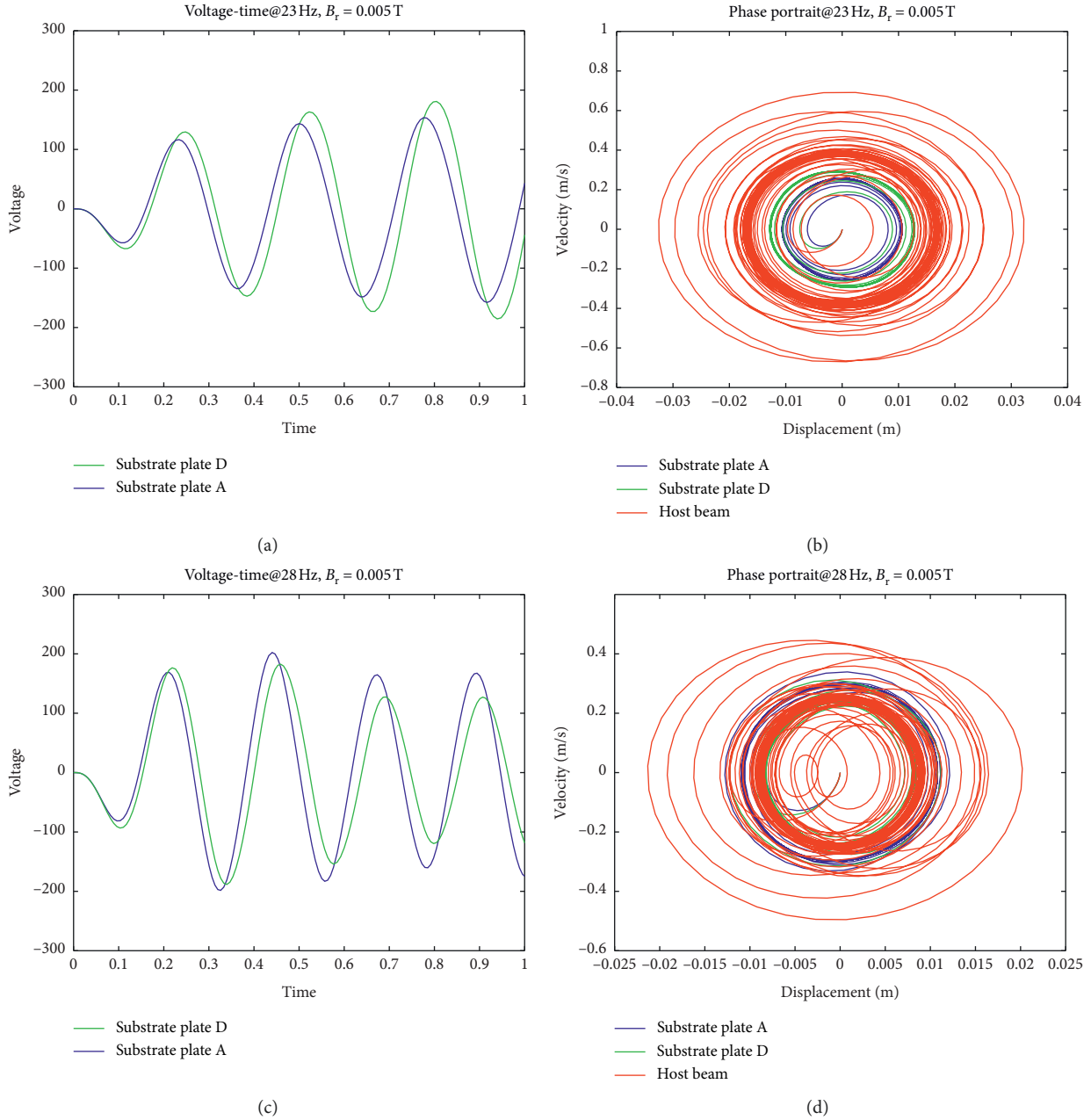

Figure 10: Continued.

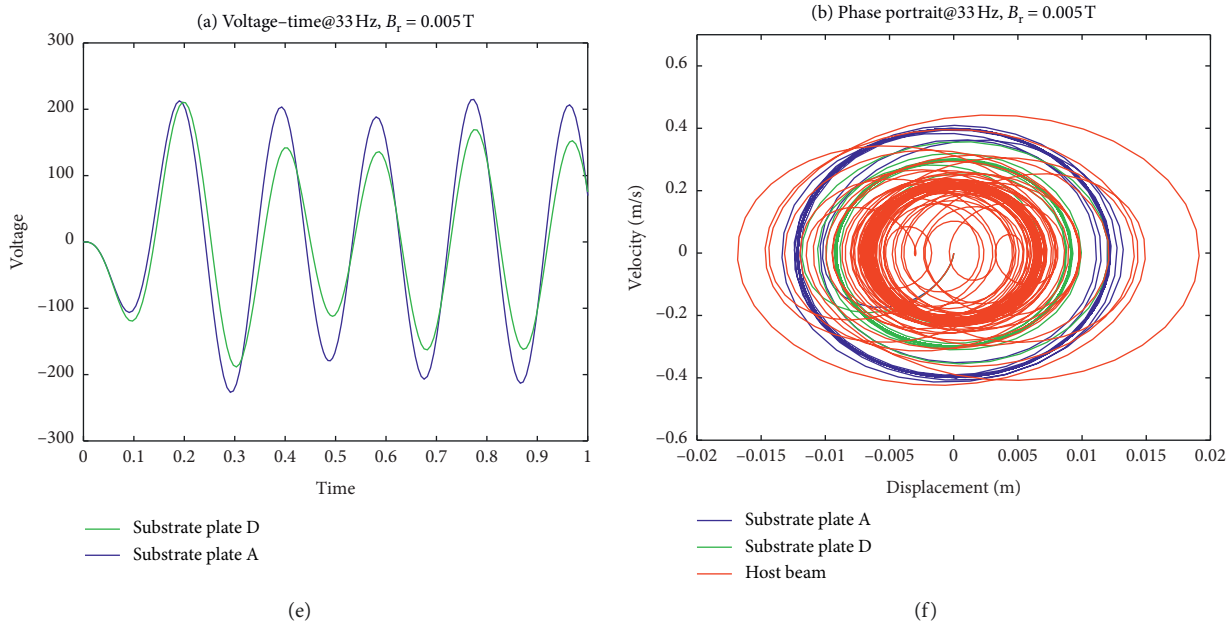

Figure 10: Voltage in time history and the phase portrait of the nonlinear EMM system: (a) voltage-time@23 Hz; (b) phase portrait@23 Hz; (c) voltage-time@28 Hz; (d) phase portrait@28 Hz; (e) voltage-time@33 Hz; (f) phase portrait@33 Hz.

Table 6: Averaged voltage (mV) of the nonlinear EMM system in 100 seconds.

	23 Hz	28 Hz	33 Hz
Substrate plate A	104.8723	110.7777	133.7134
Substrate plate D	122.0067	86.4744	99.6883
Total	226.879	197.2521	233.4017

Table 7: Averaged displacement (m) of the nonlinear EMM system in 100 seconds.

	23 Hz	28 Hz	33 Hz
Substrate plate A	0.0068	0.0068	0.0076
Substrate plate D	0.0079	0.0054	0.0057
Host beam	0.0108	0.0057	0.0042

Table 8: Averaged velocity (m/s) of the nonlinear EMM system in 100 seconds.

	23 Hz	28 Hz	33 Hz
Substrate plate A	0.1565	0.1925	0.2607
Substrate plate D	0.1898	0.1500	0.1977
Host beam	0.2437	0.1600	0.1433

In addition, the voltage produced by the baseline structure is 1.726 V@38.76 Hz as shown in Figure 12. The voltage level generated only by the piezoelectric A is similar with the baseline structure which is far less than the piezoelectric D. Therefore, the second conclusion is that the proposed piezoelectric energy harvester can generate more voltage than the baseline structure. The total voltage will be achieved at 35.54 Hz at an amplitude of the voltage of 8.133 V.

The voltage measured on the baseline structure is 1.724 V at the frequency of 38.81 Hz with only one piezoelectric layer. However, our designed harvester is comprised of two piezoelectric layers PIEZO A and PIEZO D. The voltage output has a relationship with the strains along with the piezoelectric layer. The strain has a positive relationship with the displacement of the free endpoint. Therefore, the larger the displacement, the more the voltage output on the piezoelectric layer. This is the reason why the EMM model has a total voltage of 8.133 V while the baseline only 1.724 Hz.

Figure 15 displays the comparison of power output on the designed EMM model and the baseline energy harvester. The external resistors of both devices were set up as 1 MΩ in a match with the numerical study parameters. For the EMM model, it can achieve a 66 mW at the frequency of 35.54 Hz. The baseline energy harvester only produces a 3 mW at the frequency of 38.84 Hz.

7. Summary

The design of the EMM piezoelectric vibration energy harvester system is developed from a multi-degree-of-freedom parameter model based on the cantilevered beam structure. The linear and nonlinear EMM-based energy harvesting systems are investigated and compared. The temporal voltage response and the phase portrait were studied by connecting an external circuit with a resistor to both linear and nonlinear energy harvesting systems. The results of the analytical study and the experimental validation are stated in this paper.

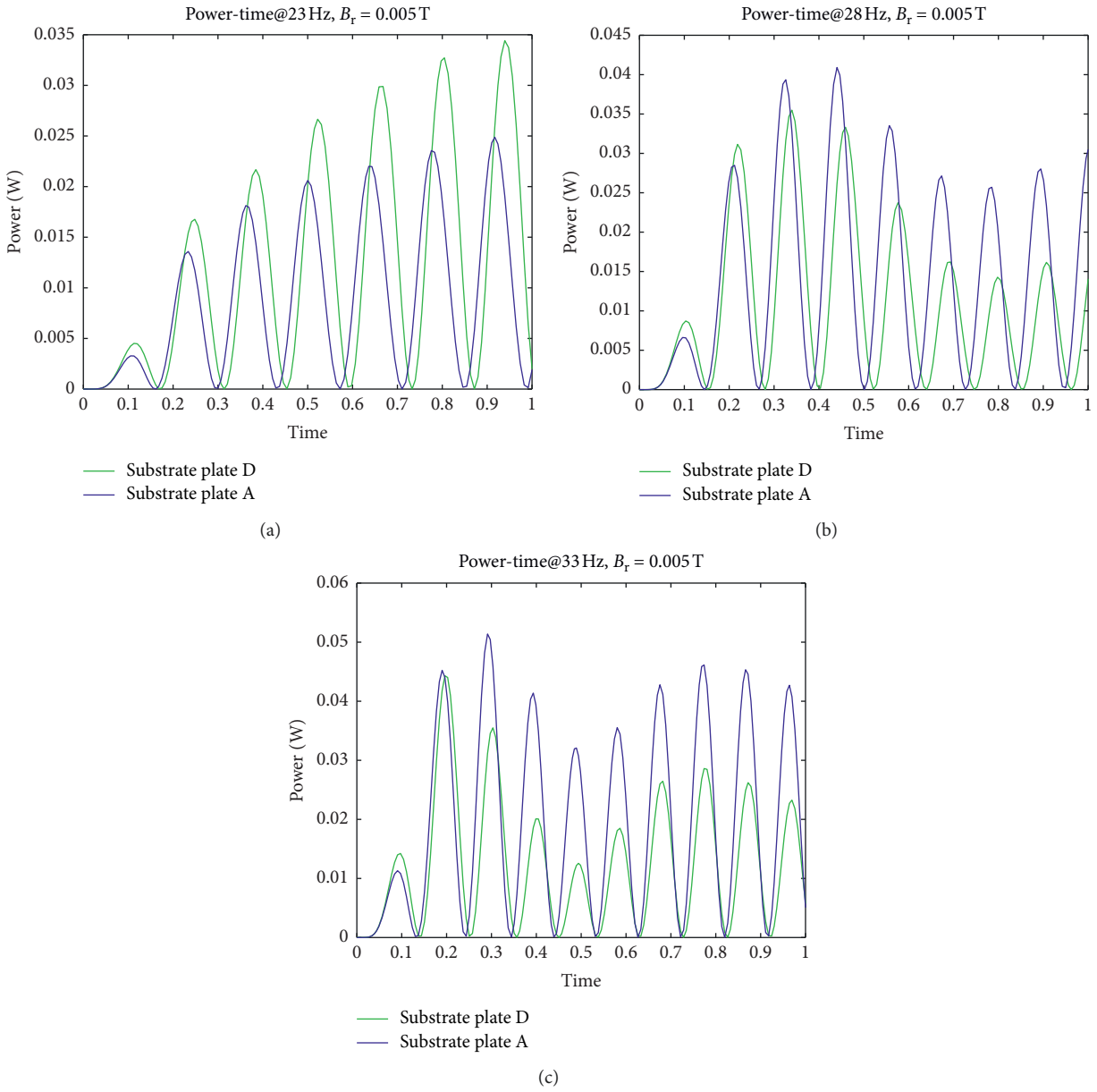

Figure 11: Power output in time history for the nonlinear EMM system: (a) 23 Hz; (b) 28 Hz; (c) 33 Hz.

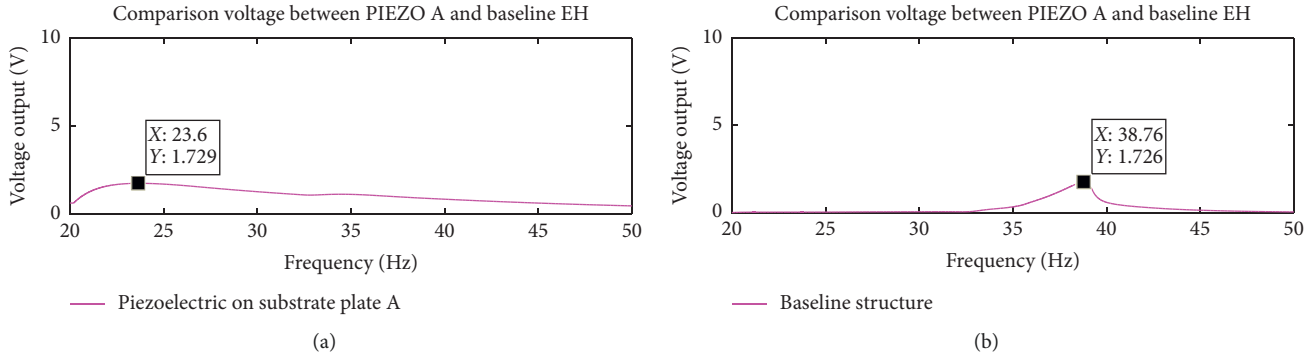

Figure 12: Voltage responses of PIEZO A and baseline EH (PIEZO A: the piezoelectric on substrate plate A; baseline EH: the baseline energy harvester).

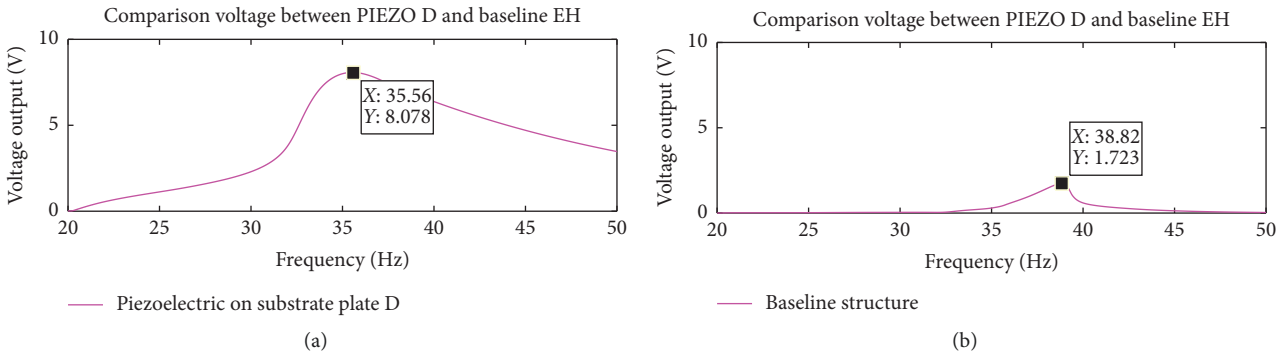

Figure 13: Voltage responses of PIEZO D and baseline EH (PIEZO D: the piezoelectric on substrate plate D; baseline EH: the baseline energy harvester).

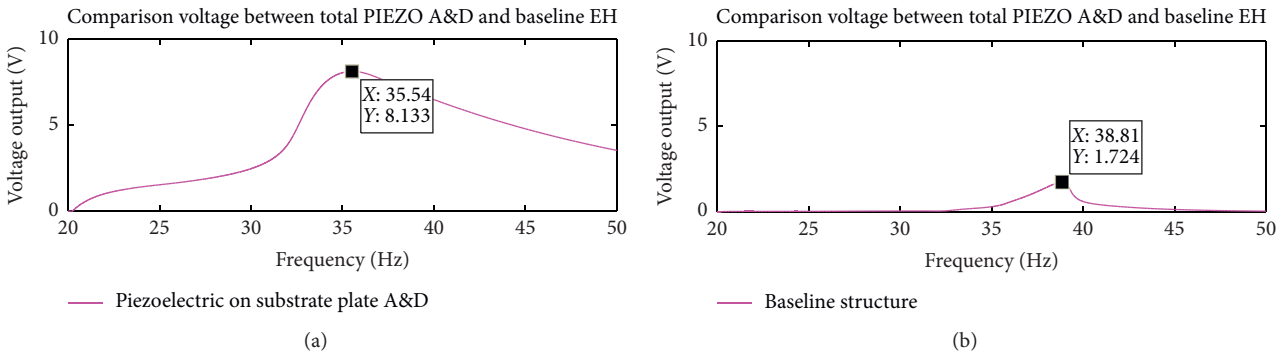

Figure 14: Voltage response between PIEZO A&D and baseline EH (PIEZO A&D: the sum of piezoelectric on substrate plate A and D; baseline EH: the baseline energy harvester).

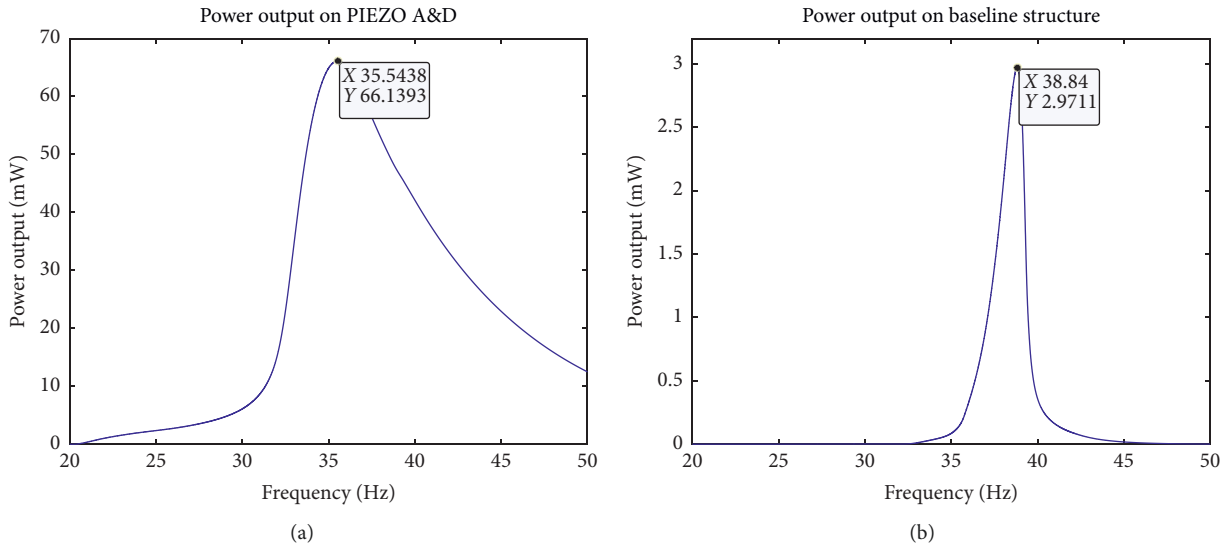

Figure 15: Comparison of power output on the designed EMM model and the baseline EH (the baseline energy harvester). (a) EMM model. (b) Baseline EH.

This paper has demonstrated that the implementation of nonlinearity built into the EMM system can change the vibration mode from a single resonance mode to two resonance modes. The EMM system has two plates, which aim at working at two vibration modes, respectively. This function of two resonance modes can enhance the energy harvester to maintain a high operating efficiency if the ability to have multiple resonance frequencies is required. The

results generated by the nonlinear EMM system show that the substrate plate D contributes 122.0067 mV at the first vibration mode of 23 Hz while the substrate plate A contributes 133.7134 V at the second vibration mode of 33 Hz. The maximum voltage yields from substrate plate D is 8.078 V@35.56 Hz and substrate plate A is 1.729 V@23.6 Hz. This characteristic guarantees the EMM-based energy harvester has a flexible and practical application because of its frequency range. Hence, the characteristic of having boarder bandwidth makes this system more flexible in absorbing the waste vibration generated by rotary machines.

In summary, this paper reports the introduction of multiple-degree-of-freedom and nonlinear structure into the design of energy harvester. The key innovation in this research work is the structure design and its nonlinearity application. There are two substrate plates which are working at different frequency ranges, respectively. The substrate plate A can work efficiently at a higher frequency range (33 Hz) while the substrate plate D can work efficiently at a relatively lower frequency (23 Hz). The flexibility in the application has been increased because of its ability in providing a broader range of resonance frequency.

Data Availability

All the data used to support the findings of this study are included within the article.

Conflicts of Interest

The authors declare that they have no conflicts of interest.

Acknowledgments

This work was supported in part by the National Natural Science Foundation of China under grant 61902437, the Fundamental Research Funds for the Central Universities, South-Central University for Nationalities under grant CZT19010, and the Research Start-up Funds of South-Central University for Nationalities under grant YZZ18006.

References

[1] F. Mansourkiaie, L. S. Ismail, T. M. Elfouly, and M. H. Ahmed, "Maximizing lifetime in wireless sensor network for structural health monitoring with and without energy harvesting," *IEEE Access*, vol. 5, pp. 2383–2395, 2017.

[2] F. K. Shaikh and S. Zeadally, "Energy harvesting in wireless sensor networks: a comprehensive review," *Renewable and Sustainable Energy Reviews*, vol. 55, pp. 1041–1054, 2016.

[3] Z. Zhang, J. Kan, S. Wang, H. Wang, C. Yang, and S. Chen, "Performance dependence on initial free-end levitation of a magnetically levitated piezoelectric vibration energy harvester with a composite cantilever beam," *IEEE Access*, vol. 5, pp. 27563–27572, 2017.

[4] M. Guan and W.-H. Liao, "Design and analysis of a piezoelectric energy harvester for rotational motion system," *Energy Conversion and Management*, vol. 111, pp. 239–244, 2016.

[5] S. P. Pellegrini, N. Tolou, M. Schenk, and J. L. Herder, "Bistable vibration energy harvesters: a review," *Journal of Intelligent Material Systems and Structures*, vol. 24, no. 11, pp. 1303–1312, 2013.

[6] T. Yildirim, M. H. Ghayesh, W. Li, and G. Alici, "A review on performance enhancement techniques for ambient vibration energy harvesters," *Renewable and Sustainable Energy Reviews*, vol. 71, pp. 435–449, 2017.

[7] A. Nammari, L. Caskey, J. Negrete, and H. Bardaweel, "Fabrication and characterization of non-resonant magneto-mechanical low-frequency vibration energy harvester," *Mechanical Systems and Signal Processing*, vol. 102, pp. 298–311, 2018.

[8] X. He, Q. Wen, Y. Sun, and Z. Wen, "A low-frequency piezoelectric-electromagnetic-triboelectric hybrid broadband vibration energy harvester," *Nano Energy*, vol. 40, pp. 300–307, 2017.

[9] D. Pan, B. Ma, and F. Dai, "Experimental investigation of broadband energy harvesting of a bi-stable composite piezoelectric plate," *Smart Materials and Structures*, vol. 26, pp. 1–14, 2017.

[10] H. Wang and L. Tang, "Modeling and experiment of bistable two-degree-of-freedom energy harvester with magnetic coupling," *Mechanical Systems and Signal Processing*, vol. 86, pp. 29–39, 2017.

[11] M. Panyam and M. F. Daqaq, "Characterizing the effective bandwidth of tri-stable energy harvesters," *Journal of Sound and Vibration*, vol. 386, pp. 336–358, 2017.

[12] J. Cao, S. Zhou, W. Wang, and J. Lin, "Influence of potential well depth on nonlinear tristable energy harvesting," *Applied Physics Letters*, vol. 106, Article ID 173903, 2015.

[13] Z. Zhou, W. Qin, and P. Zhu, "A broadband quad-stable energy harvester and its advantages over bi-stable harvester: simulation and experiment verification," *Mechanical Systems and Signal Processing*, vol. 84, pp. 158–168, 2017.

[14] Z. Zhou, W. Qin, and P. Zhu, "Improve efficiency of harvesting random energy by snap-through in a quad-stable harvester," *Sensors and Actuators A: Physical*, vol. 243, pp. 151–158, 2016.

[15] P. Kim, D. Son, and J. Seok, "Triple-well potential with a uniform depth: advantageous aspects in designing a multi-stable energy harvester," *Applied Physics Letters*, vol. 108, Article ID 243902, 2016.

[16] P. Kim and J. Seok, "A multi-stable energy harvester: dynamic modeling and bifurcation analysis," *Journal of Sound and Vibration*, vol. 333, no. 21, pp. 5525–5547, 2014.

[17] P. Kim and J. Seok, "Dynamic and energetic characteristics of a tri-stable magnetopiezoelastic energy harvester," *Mechanism and Machine Theory*, vol. 94, pp. 41–63, 2015.

[18] W. Yang and S. Towfighian, "A hybrid nonlinear vibration energy harvester," *Mechanical Systems and Signal Processing*, vol. 90, pp. 317–333, 2017.

[19] J. Jung, P. Kim, J.-I. Lee, and J. Seok, "Nonlinear dynamic and energetic characteristics of piezoelectric energy harvester with two rotatable external magnets," *International Journal of Mechanical Sciences*, vol. 92, pp. 206–222, 2015.

[20] Z. Chen, B. Guo, C. Cheng, H. Shi, and Y. Yang, "Chaotic dynamics-based analysis of broadband piezoelectric vibration energy harvesting enhanced by using nonlinearity," *Shock and Vibration*, vol. 2016, Article ID 3584740, 11 pages, 2016.

[21] L. Tang and Y. Yang, "A multiple-degree-of-freedom piezoelectric energy harvesting model," *Journal of Intelligent Material Systems and Structures*, vol. 23, no. 14, pp. 1631–1647, 2012.

[22] K. Tao, J. Wu, L. Tang et al., "A novel two-degree-of-freedom MEMS electromagnetic vibration energy harvester," *Journal*

of Micromechanics and Microengineering, vol. 26, no. 3, Article ID 035020, 2016.

[23] A. Čeponis and D. Mažeika, "Investigation of multifrequency piezoelectric energy harvester," *Shock and Vibration*, vol. 2017, Article ID 8703680, 13 pages, 2017.

[24] S. Zhou, J. Cao, W. Wang, S. Liu, and J. Lin, "Modeling and experimental verification of doubly nonlinear magnet-coupled piezoelectric energy harvesting from ambient vibration," *Smart Materials and Structures*, vol. 24, no. 5, Article ID 055008, 2015.

[25] Z. Chen, B. Guo, Y. Xiong, C. Cheng, and Y. Yang, "Melnikov-method-based broadband mechanism and necessary conditions of nonlinear rotating energy harvesting using piezoelectric beam," *Journal of Intelligent Material Systems and Structures*, vol. 27, no. 18, pp. 2555–2567, 2016.

[26] Y. J. Gao, Y. G. Leng, S. B. Fan, and Z. H. Lai, "Performance of bistable piezoelectric cantilever vibration energy harvesters with an elastic support external magnet," *Smart Materials and Structures*, vol. 23, no. 9, Article ID 095003, 2014.

[27] X. D. Xie, Q. Wang, and N. Wu, "A ring piezoelectric energy harvester excited by magnetic forces," *International Journal of Engineering Science*, vol. 77, pp. 71–78, 2014.

[28] H.-Y. Wang, L.-H. Tang, Y. Guo, X.-B. Shan, and T. Xie, "A 2DOF hybrid energy harvester based on combined piezoelectric and electromagnetic conversion mechanisms," *Journal of Zhejiang University SCIENCE A*, vol. 15, no. 9, pp. 711–722, 2014.

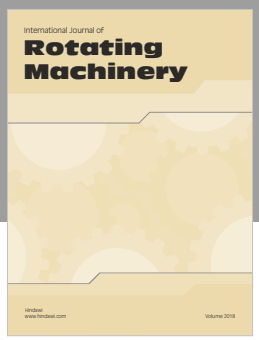

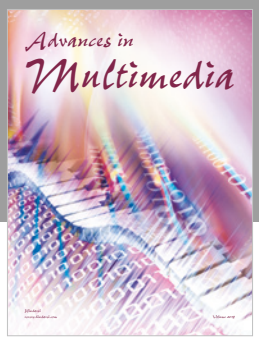

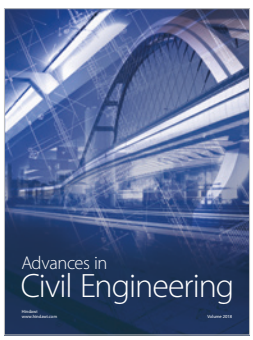

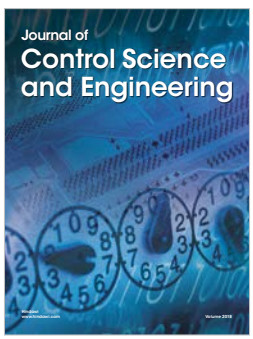

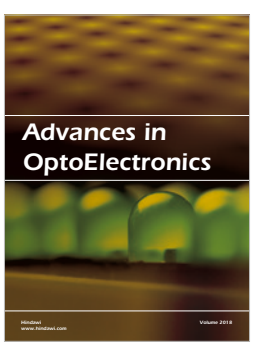

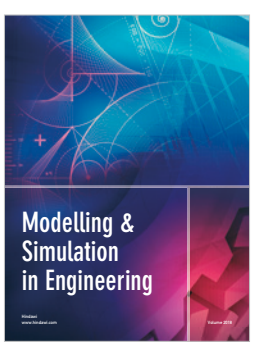

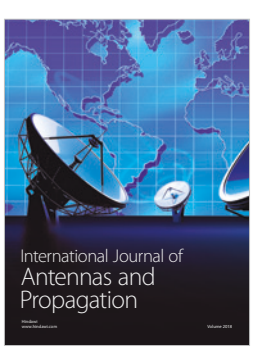

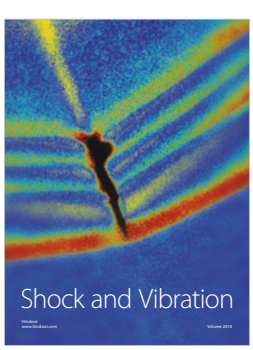

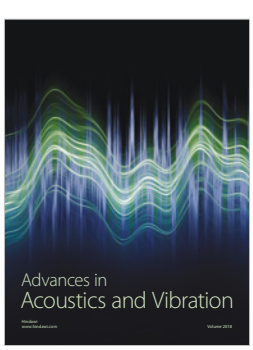

Hindawi

Submit your manuscripts at
www.hindawi.com